9372–9387 *Nucleic Acids Research, 2017, Vol. 45, No. 16* *Published online 27 June 2017*
doi: 10.1093/nar/gkx562

Regulation of chromatin folding by conformational variations of nucleosome linker DNA

Jenna M. Buckwalter[1], Davood Norouzi[2], Anna Harutyunyan[1], Victor B. Zhurkin[2,*] and Sergei A. Grigoryev[1,*]

[1]Penn State University College of Medicine, Department of Biochemistry and Molecular Biology, H171, Milton S. Hershey Medical Center, P.O. Box 850, 500 University Drive, Hershey, PA 17033, USA and [2]Laboratory of Cell Biology, CCR, National Cancer Institute, NIH, Bethesda, MD 20892, USA

Received March 08, 2017; Revised May 30, 2017; Editorial Decision June 15, 2017; Accepted June 19, 2017

ABSTRACT

Linker DNA conformational variability has been proposed to direct nucleosome array folding into more or less compact chromatin fibers but direct experimental evidence for such models are lacking. Here, we tested this hypothesis by designing nucleosome arrays with A-tracts at specific locations in the nucleosome linkers to induce inward (AT-IN) and outward (AT-OUT) bending of the linker DNA. Using electron microscopy and analytical centrifugation techniques, we observed spontaneous folding of AT-IN nucleosome arrays into highly compact structures, comparable to those induced by linker histone H1. In contrast, AT-OUT nucleosome arrays formed less compact structures with decreased nucleosome interactions similar to wild-type nucleosome arrays. Adding linker histone H1 further increased compaction of the A-tract arrays while maintaining structural differences between them. Furthermore, restriction nuclease digestion revealed a strongly reduced accessibility of nucleosome linkers in the compact AT-IN arrays. Electron microscopy analysis and 3D computational Monte Carlo simulations are consistent with a profound zigzag linker DNA configuration and closer nucleosome proximity in the AT-IN arrays due to inward linker DNA bending. We propose that the evolutionary preferred positioning of A-tracts in DNA linkers may control chromatin higher-order folding and thus influence cellular processes such as gene expression, transcription and DNA repair.

INTRODUCTION

In eukaryotic cells, DNA is organized into chromatin via a hierarchical structure. The primary level consists of nucleosome core particles, the basic repeat until of chromatin, involving ∼147 base pairs (bp) of DNA wrapped around an octamer of core histones (1). Consecutive nucleosome cores are connected by linker DNA, 10–70 bp in length, forming nucleosome arrays that are further compacted into higher-order chromatin fibers with the aid of linker histone, monovalent and divalent cations, histone tail modifications, chromatin architectural proteins and nucleosome–nucleosome interactions (2–6). The compactness of the chromatin higher-order fibers distinguishes the organization of gene-poor heterochromatin from gene-rich, transcriptionally active euchromatin (7) and may directly control nucleosomal access for pioneer DNA-interacting transcriptional factors (8).

The structure of the nucleosome is relatively uniform and known at atomic resolution (1,9) and several competing models have been proposed for folding of nucleosome arrays into the so-called 30-nm fibers, the predominant form of higher-order chromatin observed *in vitro* (10–12). Experimental techniques using *in situ* preparations (13), chromatin isolated from various cell types and reconstituted nucleosome arrays have provided experimental evidence on which these models are based. The principal difference between the models is the geometry of nucleosome linker DNA being either straight or bent and thus, changing the orientation of nucleosome and inter-nucleosome interactions. The solenoid models indicate chromatin compaction is achieved by regular coiling of linker DNA along the superhelical path in the nucleosome core to make a regular 1-start helix and results in neighboring nucleosomes making face-to-face contacts (14,15). Alternatively, the zigzag helical models include a 2-start order of the nucleosome stacking with nucleosome linkers in an extended conformation crossing the main fiber axis (16). Electron microscopy studies of nucleosome arrays reconstituted from tandem repeats of nucleosome positioning sequence provide a decisive support for the zigzag organization of the 30-nm fiber (17–19). However, the linker DNA conformation appears to not follow the ideal path predicted by the regular helical models. In

*To whom correspondence should be addressed. Tel: +1 717 531 8588; Fax: +1 717 531 7072; Email: sag17@psu.edu
Correspondence may also be addressed to Victor B. Zhurkin. Tel: +1 240 760 7244; Fax: +1 301 402 4724; Email: zhurkin@nih.gov

particular, the X-ray crystal structure of a tetranucleosome at 9 Å resolution showed linker DNA that zigzagged back and forth between two stacks of nucleosome cores containing partially bent linkers (20). Our work, using electron microscopy-assisted nucleosome interaction capture (EMANIC) and modeling, showed that straight linkers can coexist with bent linkers within the same nucleosome arrays (21). Furthermore, the internucleosomal interaction pattern within the interphase chromatin *in situ* suggests preservation of the overall zigzag configuration *in situ* without forming regular helical repeats (22,23). With the use of modeling approaches, it was suggested that chromatin structure and interactions between remote nucleosomes are strongly influenced by the variable length and conformation of linker DNA (21,24–31).

Here, we investigated the role of linker DNA conformational variability using the well-known fact that short DNA sequences of A:T base pairs (A-tracts) induce anisotropic bending in DNA up to ∼20° (32,33) and are found at high frequencies in linker DNA regions (34). We show that A-tracts induce bending in nucleosome linker DNA that directly impacts chromatin higher-order structures. Furthermore, we demonstrate that the location of the A-tracts relative to the nucleosome core-linker boundary alters the resulting nucleosome–nucleosome interactions and thus contributes to the extent in which the chromatin is compact. Altogether, our results suggest that linker DNA sequence may play an important role in linker DNA conformation that could impact not only local chromatin structure but also regulation of chromatin-based processes by modulating nucleosome positioning and chromatin folding.

MATERIALS AND METHODS

Nucleosome positioning templates and arrays

Using clone 601 DNA (35), DNA templates were designed to position nucleosome with single-nucleotide precision, and specific DNA sequences were added to the linker DNA (Figure 1D and Supplementary Figure S1). A 188-bp monomer DNA (29) was used as the template and A-tracts as well as restriction enzyme sites were incorporated through primer modification polymerase chain reaction (PCR). Every monomeric template was designed with an XbaI restriction site at the 5′-end and SpeI and SphI sites at the 3′-end. Using XbaI and SphI, all monomeric templates were ligated into pUC19 vector, transformed into *Escherichia coli* DH5α (Invitrogen, # 18265017), and grown in the presence of carbenicillin. Expansion to 12-mer and 24-mer templates was done using a step-by-step method in which plasmids were digested with SpeI and SphI to yield linearized vectors containing monomers, or XbaI and SphI to yield monomeric inserts. Ligation of the monomeric insert to the vector containing a monomeric positioning template resulted in ligation of XbaI and SpeI sites eliminating the site and yields a dimer or two nucleosome positioning templates in one vector. This process was repeated until constructs contained 12 or 24 positioning templates.

The finished DNA templates constructed in pUC19 plasmids were then transformed and grown in 5 l of media. The large-scaled alkaline lysis procedures (36) were used to isolate the plasmids. All our plasmids were digested from the vector backbone using XbaI and HindIII sites while the vector backbone was digested into smaller fragments using DraI (1120, 862, 692, 19 bp) to serve as carrier DNA (oligonucleosome array reconstitution).

Histone octamer isolation and purification

Core histone octamers were isolated from chicken erythrocyte nuclei using ultracentrifugation under increasing ionic strength as described (21). Core histones were further purified using FPLC and a HiLoad™ 16/60 Superdex™ 75 prep grade column. The column was equilibrated with core histone isolation buffer (2 M NaCl, 10 mM Tris pH 7.6, 1 mM ethylenediaminetetraacetic acid (EDTA), 5 mM β-ME) that was purified using a 0.2 μ filter. The concentrated core histones were loaded on the column (2 ml per run) at a flow rate of 0.5 ml/min collecting 2 ml fractions. The UV readings were used to determine the fractions that contained histones and were analyzed by sodium dodecyl sulphate-polyacrylamide gel electrophoresis (SDS-PAGE). Fractions containing equimolar amounts of core histone proteins were stored at −20°C.

Linker histone isolation

The supernatant from the 0.65-M centrifugation step from the core histone isolation procedure was used to isolate linker histone H1. The 0.65 M NaCl supernatant solution was diluted to 0.3 M NaCl using Buffer A (20 mM HEPES pH 7.5, 50 mM NaCl, 0.02% sodium azide) and 0.5 mM Phenylmethylsulfonyl Fluoride (PMSF). A 1 ml HighTrap SpHp ion exchange column (GE Healthcare) was equilibrated with Buffer A. The supernatant was loaded into a 50 ml superloop and applied to the column. Linker histone H1 was eluted using a two-step gradient of Buffer B (20 mM HEPES, 1.5 M NaCl, 0.02% sodium azide) with a flow rate of 0.5 ml/min, and linear gradients from 0–33% Buffer B over 2.5 column volumes and 33–100% Buffer B over 35 column volumes. The resulting fractions were analyzed by SDS-PAGE, and fractions containing linker histone H1 were aliquoted and stored at −80°C. The concentration of linker histone was determined using densitometry analysis (37).

Oligonucleosome array reconstitution

Reconstitution of 12-mer and 24-mer templates (described above) with chicken erythrocyte histones were performed as described in (38) but in the presence of carrier DNA (39) to ensure proper loading. Carrier DNA was generated through digestion of pUC19 with DraI and used at a ratio of 2:1 with template DNA. Core histones and DNA were combined in a mixture that contained a final concentration of 2M NaCl and 1 mM PMSF. Using 3500 molecular weight cut-off (MWCO) membranes, samples were dialyzed against buffer (2M NaCl, 10 mM HEPES, 0.2 mM EDTA, 0.1% NP-40, 5 mM β-ME, pH = 7.5) for 2 h at 4°C. The salt concentration was lowered continuously thereafter (all other buffer component concentrations remained the same) to 1.5 M NaCl for 2 h, 1 M NaCl for 3 h and 0.75 M NaCl for 3 h. The salt concentration was decreased to

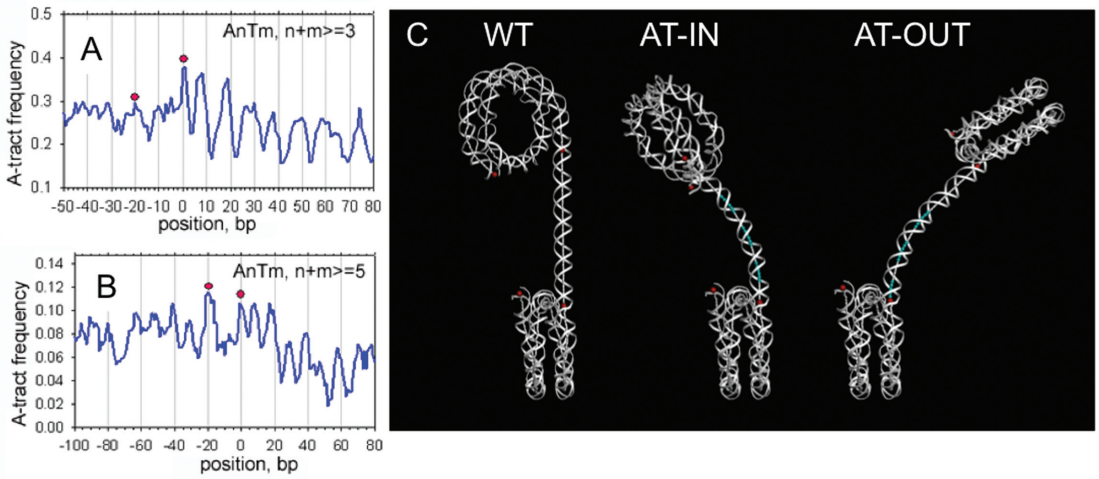

D

Construct	Linker DNA Sequence
Wild-type	TGCATGTGGATCCGAATTCATACTAGACTATACGCGGCCGCCCTGGAGAATC...
AT-IN	CTGCATGACTAGACAAAAAACCGGAAAAAACCGGAAAAATGCCCTGGAGAATC...
AT-OUT	CTGCATGACTAGAACCCGGAAAAAACCGGAAAAAACCGGCAAAAATGAGAATC...
	| | | | | | | | | |
	-40 -35 -30 -25 -20 -15 -10 -5 0 +5

Figure 1. Design and construction of oligonucleosome arrays with directed linker DNA bending. (**A** and **B**) Frequencies of occurrence of (A) short A-tracts (A_nT_m, n+m ≥ 3) and (B) long A-tracts (A_nT_m, n+m ≥ 5) in the cores and flanking regions of chicken nucleosomes. The frequencies are 'symmetrized' with respect to the dyad at position 74 (data from (34)). (**C**) Models of WT and A-tract containing nucleosome dimers based on X-ray crystal structure of clone 601 mononucleosome with 145 bp core (3MVD, (44)) and 43 (WT) or 44 (AT-IN and AT-OUT) bp linker DNA shown in (**D**) and Supplementary Figure S1. (D) Linker DNA sequences of the oligonucleosome constructs. Wild-type (WT) linkers have no specific DNA sequence while AT-IN linkers have A-tracts located at −5, −15, −25 in relation to the nucleosome binding core and AT-OUT linkers have A-tracts located at 0, −10, −20 in relation to the nucleosome binding core. Sequence numbering is according to (51). The term 'inward' bending of the linker DNA (AT-IN) describes a trajectory toward the nucleosome core dyad axis and the 'outward' bending (AT-OUT)—a trajectory away from the dyad axis.

0.5 M NaCl and dialyzed overnight (∼18 h). Reconstitutes were then dialyzed for 3 h against a buffer containing 5 mM NaCl, 10 mM HEPES, 0.2 mM EDTA, 0.1% NP-40, 5 mM β-ME, pH = 7.5 for 3 h then switched to a buffer containing all the same components except NP-40. Reconstitutes were quantified by spectrophotometry (A260 nm) measurements and visualized on 1% Type IV agarose deoxynucleoprotein (DNP) gels run at 80 V/cm in HE buffer (20 mM HEPES, 0.1 mM EDTA). Reconstitutes were also digested with restriction enzymes (AT-IN, AT-OUT: MspI; WT: BamHI) to ensure proper histone loading (Supplementary Figure S3). Reconstitutes were also assayed through SDS-PAGE to verify integrity of core histones.

In cases where core arrays were reconstituted with linker histone, core arrays were mixed with linker histone H1 at a molar ratio of one molecule of H1 per nucleosome. The first dialysis step was against a buffer containing 500 mM NaCl, 10 mM HEPES, 0.1 mM EDTA, 0.025% NP-40, pH = 7.5 using 3500 MWCO membranes at 4°C for 2 h followed by an overnight dialysis (∼18 h) against 5 mM NaCl, 10 mM HEPES, 0.1 mM EDTA, 0.025% NP-40, pH = 7.5 buffer. The reconstitutes were dialyzed for 4 h against 5 mM NaCl, 10 mM HEPES, 0.1 mM EDTA, pH = 7.5 to remove NP-40. After dialysis, 0.1 mM PMSF was added and samples were quantified using A_{260} readings then stored at 4°C.

The removal of carrier DNA post-reconstitution by purifying reconstitutes on a 5–25% sucrose gradient in buffer containing 10 mM Tris, 1 mM EDTA, 0.5 mM PMSF and centrifuged at 35 000 RPM at 4C for 8 h (12-mers) or 4 h (24-mers) on the ultracentrifuge in the Beckman SW41Ti swinging bucket rotor. After centrifugation, ∼1 ml fractions were removed top to bottom on the sucrose gradient using Auto Densi-Flow (115V) machine and analyzed on 0.8% Type IV agarose gel (d) run at 80 V/cm in HE buffer for ∼1 h. Fractions containing arrays without carrier were dialyzed against 10 mM HEPES, 5 mM NaCl, 0.1 mM EDTA, pH = 7.5, for ∼36 h to remove sucrose. Analysis using SDS-PAGE confirmed integrity of core histones.

Analytical ultracentrifugation

Assaying the extent of nucleosome array folding via sedimentation velocity experiments was performed on the analytical ultracentrifuge (Beckman Optima XL-A) (40). Chromatin arrays were run in HEPES-NaCl-EDTA (HNE) buffer containing 10 mM HEPES, 0.1 mM EDTA, pH 7.5 under varying ionic strength conditions (5 mM, 150 mM NaCl, 1 mM $MgCl_2$ and 150 mM plus 1 mM $MgCl_2$) at a concentration of A_{260} = 0.5 OD. Scan data were collected using ProteomeLab XL-A, at a wavelength of 260 nm while samples were spun at 20000 RPM for ∼3 h at 20°C. Analytical ultracentrifuge data was analyzed using the continuous c(S) distribution model of SEDFIT software (41) (http://www.analyticalultracentrifugation.com).

Restriction enzyme digestion assay

AT-IN and AT-OUT 24-mer core arrays were diluted to 10 μg/ml in a 1 ml reaction media containing 150 mM NaCl and diluted restriction enzyme digested buffer (1.25 mM potassium acetate, 0.5 mM Tris acetate, 0.25 mM magnesium acetate, 2.5 μg/ml bovine serum albumin). Six units of MspI restriction enzyme (Thermo Scientific, FD0544) was added, the reaction mixture was incubated at +37°C and the enzymatic reaction was quenched at the specified time points using a final concentration of 10 mM EDTA. The digested core arrays were treated with SDS and Proteinase K at 55°C for 1 h and DNA purified using Wizard SV Gel and PCR Clean-Up System (Promega A9281). Samples were quantified and 500 ng of DNA from each time point was run on a Type I agarose gel in Tris-acetate-EDTA (TAE) buffer for 4 h at 80 V/cm in a horizontal gel electrophoresis apparatus with constant buffer recirculation (Fisher, FB-SBR-1360). The gels were stained by Ethidium Bromide, visualized using Bio-Rad Gel Doc Molecular Imager. The images were saved as tiff files, then scanned and analyzed by ImageJ software to determine the relative intensity of each band as the percent of intact band. DNA accessibility was measured as the rates of cleavage of nucleosomal DNA relative to cleavage of naked DNA as described (42).

Electron microscopy and EMANIC

For electron microscopy imaging, the reconstituted arrays with DNA concentration ∼50 μg/ml were incubated in HNE (10 mM HEPES, 5 mM NaCl, 0.1 mM EDTA, pH.7.5) buffer with specified salt conditions (e.g. 5 mM NaCl, 150 mM NaCl or 1 mM $MgCl_2$) for 1 h. For direct transmission electron microscopy (TEM), the samples were fixed by adding 0.1% glutaraldehyde at 4°C for 5 h, followed by 12-h dialysis against HNE buffer in 10 000 MWCO membrane dialysis cups at 4°C. For EMANIC (21), the samples were brought to room temperature, 0.08% formaldehyde (ACS reagent; Fisher) was added, samples were incubated at room temperature for 5 min and the reactions were quenched by adding starting reaction media (without formaldehyde) containing 100 mM glycine, pH 7.8, to final concentration of 40 mM and cooling on ice. The samples were dialyzed for 5 h against 10 mM Na-borate, pH 9.0, 0.1 mM EDTA and then for 12 h against HNE in 10 000 MWCO membrane dialysis cups at 4°C. The dialyzed samples (both TEM and EMANIC) were diluted about 50-fold with 50 mM NaCl to 50 μg/ml final concentration and applied to carbon-coated and glow-discharged EM grids (T1000-Cu, Electron Microscopy Sciences), and stained with 0.04% uranyl acetate. Dark-field EM imaging was conducted as before (21) at 120 kV using JEM-1400 electron microscope (JEOL USA, Peabody, MA, USA) with SC1000 ORIUS 11 megapixel CCD camera (Gatan Inc. Warrendale, PA, USA).

For EMANIC, EM images were collected at 25K magnification. For each sample, nucleosomal arrays containing 12 distinguishable nucleosome cores were selected to score internucleosomal interactions. Minimum 1500 (average 2130) nucleosomes were scored for each sample (Supplementary Table S1). Individual nucleosomes were overlaid with masks of nucleosome-size disks that were scaled to diameter of 110 Å for each given magnification, centered over each nucleosome and connected with lines tracing the underlying linker DNA. Internucleosomal interactions were scored as positive if the scaled nucleosome disks contacted each other. In the rare cases when the crosslinked array contained more than one loop razing the possibility of ambiguous loop assignment, to minimize the possible error we uniformly accounted for all alternative configurations and selected the one with minimal sum of nucleosomes in the loops. Images of all control and crosslinked WT, IN and OUT arrays overlaid with scoring masks for EMANIC are shown in Supplementary EM imaging data files (filenames are listed in Supplementary Table S1). Standard deviations were obtained from at least three EM experiments; *P*-values (see Supplementary Table S2) represent probability associated with a Student's two-sample *t*-test with a two-tailed distribution.

Mg^{++}-dependent chromatin self-association assays

The extent of chromatin self-association was analyzed using selective precipitation in magnesium similar to (43). 12-mer nucleosome arrays with $A_{260nm} = 0.5$ were incubated with increasing concentrations of $MgCl_2$ (Sigma Aldrich, #M1028–1 ml) for 20 min on ice. The reactions were then centrifuged at 12 000 rpm, 4°C, for 10 min. Supernatants were collected first, then the pellets were resuspended in 25% glycerol, 50 mM EDTA, 0.5% SDS. DNA from supernatants and pellets were analyzed on a 1% agarose gel and stained with Ethidium Bromide. The percentage of DNA in the supernatant was determined by DNA band quantification using Image J software. The concentration of $MgCl_2$ at which 50% of the reconstituted chromatin was precipitated was recorded.

3D computational modeling

Starting configurations of the three types of nucleosome arrays (WT, IN and OUT) consisting of 12 identical sequential nucleosome-linker units were constructed as described before (27). The nucleosome core sequence (145 bp) in all three constructs is the Widom's clone 601 sequence (Supplementary Figure S1); the structure of the nucleosome core has been solved by X-ray crystallography (PDB ID: 3mvd (44)). This part is assumed fixed during simulation and only goes through rigid body motions. The linker DNA sequences for WT, IN and OUT are given in Figure 1D.

The DNA is modeled at the level of dimeric steps, and its trajectory is described by the six base-pair step parameters (45). Geometry of the linker DNA fluctuates around the regular B-DNA except at the A-tracts. Regular B-DNA parameters are [Twist, Tilt, Roll, Shift, Slide, Rise] = [34.5°, 0, 0, 0, 0, 3.35 Å] on average. A-tracts have a different set of average parameters [Twist, Tilt, Roll, Shift, Slide, Rise] = [37°, 0, −5°, 0, 0, 3.35 Å], with an increased Twist and a moderate bend into the minor groove (46). We used the following four energy terms: elastic, electrostatic, histone H4 tail–acidic patch interactions and the steric hindrance terms (27) as specified:

i. The elastic energy of the linker DNA deformations is calculated using the knowledge-based potential functions (45).

ii. The electrostatic energy is calculated using the Coulomb potential with 30 Å cutoff. The DNA charges are partially neutralized due to the salt screening effect.
iii. Stacking or the H4 tail—acidic patch interactions are modeled phenomenologically, with the minimum of the inter-nucleosome interaction either −8 kT (27) or −2.7 kT (47) and a 35 Å range of action.
iv. Steric clashes are modeled by a van der Waals-like repulsion potential.

A single simulation step of the classical Monte Carlo (MC) procedure entails the following:

i. random selection of a DNA base-pair step in one of the linkers and alteration of its six parameters by addition of a random perturbation;
ii. calculation of 'new' positions of all 12 nucleosomes and 11 linkers in the nucleosome array;
iii. computation of the energy and performance of the Metropolis acceptance test (48).

After every 5000 successful MC steps the 12-mer array conformations were saved (denoted as snapshots). Statistical averaging of various parameters of the system (e.g. sedimentation coefficient) was performed for 10 000 snapshots taken after the system was equilibrated. For any selected conformation of oligo-nucleosomal array, the sedimentation coefficient $s_{20,w}$° was calculated as described (49).

RESULTS

Nucleosome array folding reflects the intrinsic nature of the linker DNA sequence

Design of linker DNA sequence was based on both structural and biological considerations. Previous analysis of nucleosome positioning data bases, which indicated enrichment of A-tracts in linker DNA regions, noted high frequency of A-tracts at positions 0 and −20 in relation to the nucleosome core-linker boundary (Figure 1A and B) (34). Thus, the linker DNA is likely to be bent into the minor groove at these positions (32,50). Interestingly, in the crystal structure of tetranucleosome (20), one linker is straight and two linkers are notably bent into the minor groove at position −10, that is, in the same rotational setting relative to the nucleosome core-linker boundary. Accordingly, in one of our constructs the A-tracts were inserted at positions 0, −10 and −20 (Figure 1D). In such a case, our model predicts that the A-tracts will promote outward bending of the nucleosome linker (Figure 1C)—therefore, this construct is denoted AT-OUT. The second construct, AT-IN, contains A-tracts at positions −5, −15 and −25 (Figure 1D), which have the opposite rotational setting and are expected to produce inward bending of the nucleosome linker (Figure 1C) and ultimately influence the folding of nucleosome arrays. The control construct, WT, contains no repeated nucleotide tracts (Figure 1D) and was used in our previous reconstitution experiments (29). The predicted linker DNA lengths are 44 bp for the AT-IN and AT-OUT constructs and 43 bp for the WT construct based on the 145 bp clone 601 nucleosome core (44,51), see Supplementary Figure S1.

Reconstituted nucleosome arrays with specific linker DNA sequences were assembled using the clone 601 sequence (35) and histone octamers isolated from chicken erythrocyte nuclei. Reconstitutes with chicken erythrocyte histones have been widely used in chromatin higher-order studies such as sedimentation velocity (40), self-association (43) and EM (21,29,39) thus providing reference datasets and quality controls. Also, chicken erythrocyte histones produce nucleosome crystals whose x-ray structure is similar to that of recombinant histones (52).

Precise histone stoichiometry is crucial for proper folding of nucleosome arrays and several independent approaches were used to analyze histone loading of each array. First, analysis of the reconstitutes on agarose DNP gels is ideal for oligonucleosome separation where smearing of carrier DNA indicated that high affinity (clone 601) templates had been saturated with histone octamers and excess histones were bound to the low-affinity carrier DNA (Supplementary Figure S2A and B). In this instance, the band-shifts of the carrier DNA and the absence of additional self-associated bands of the nucleosome arrays indicates the optimal loading of histone octamers without over-saturation (29). Secondly, reconstituted nucleosome arrays were digested with restriction enzymes into mononucleosomes and analyzed on DNP gels in TAE buffer optimized for resolving mononucleosomes and free DNA (see design scheme of constructs on Supplementary Figure S3A). The resulting digest pattern was indicative of the efficiency of histone loading on the clone 601 templates where the absence of free DNA indicated fully loaded material (Supplementary Figure S3B and C). Samples with optimal DNA to core histone ratio were reconstituted at a larger scale and purified on sucrose gradients to isolate optimally loaded arrays from carrier DNA with a yield of ∼100 μg DNA. Using TEM of nucleosomes arrays unfolded at low ionic strength, expected nucleosome numbers in most nucleosome arrays was confirmed by detecting the predicted number of nucleosomes per array (Supplementary Figure S2C–E); the presence of about 20% arrays with less than 12 nucleosomes and about 10% arrays with more than 12 nucleosomes is consistent with our previous estimation for a series of nucleosome arrays with WT linkers (29) indicating that adding of A-tracts does not affect clone 601 reconstitution with histones.

Mg^{++}-dependent self-association (43) was used to assay the extent to which chromatin arrays self-associate or form tertiary structures. The self-association of 12-mer arrays was measured by recording the concentration of $MgCl_2$ at which 50% of the reconstituted chromatin was precipitated. Changes in linker DNA sequence resulted in notable changes in the rate of self-association between AT-track containing nucleosome arrays and WT arrays as both AT-IN and AT-OUT constructs had lower 50% precipitation points (1.6 mM for AT-OUT; 1.9 mM for AT-IN) compared to WT (2.1 mM) by ∼ 1 mM $MgCl_2$ (Supplementary Figure S2F). At the same time, no significant differences between AT-IN and AT-OUT were observed. These results indicate that the anisotropic positioning of the A-tracts in linker DNA does not significantly affect the tertiary level of chromatin higher-order structure.

Adenine tracts in linker DNA alter nucleosome array folding by inward and outward bending of nucleosome linkers

We constructed and characterized a series of nucleosome core arrays in which the nucleosome linker contained A-tracts at specific locations relative to the nucleosome binding site expected to induce anisotropic bending in the nucleosome linker as well as a control construct with no specific sequence in the nucleosome linker (wild-type, WT). As such, reconstituted 12-mer chromatin arrays were assembled with nucleosome linkers containing A-tracts to induce inward (AT-IN) or outward (AT-OUT) bending of nucleosome linkers. The extent of nucleosome array folding for arrays with different linker DNA sequences were assayed by sedimentation velocity analysis using the continuous c(S) distribution model (41). The homogeneity of samples was confirmed by sharp peaks observed when analyzing sedimentation data. Due to the continuous c(S) distribution model's capabilities of indicating homogeneity and heterogeneity of nucleosome arrays (29), we used this model throughout this work. Under low ionic conditions (5 mM NaCl), the sedimentation peaks observed had very similar distributions of sedimentation coefficients around 30 S with AT-IN showing the slowest sedimentation (∼26 S) (Figure 2A).

TEM imaging was used to confirm results of sedimentation velocity experiments. The 12-mer WT, AT-IN, and AT-OUT arrays were fixed at low ionic conditions (5 mM NaCl) and imaged. Here, we observed a 'beads-on-a-string' conformation as expected for AT-IN and AT-OUT. Interestingly, in addition to sedimentation velocity showing the lowest sedimentation rates for AT-IN (Figure 2A), TEM images showed AT-IN 'beads-on-a-string' to be somewhat more kinky than AT-OUT (Figure 2B). The slightly lower sedimentation rates of the unfolded AT-IN suggest that this kinky AT-IN conformation provides more friction during sedimentation thus reducing sedimentation velocity.

Upon the induction of chromatin folding by 150 mM NaCl, we observed a noticeable increase in sedimentation velocity for all samples (Figure 2C and D). Notably, the salt-dependent increase was greatest for AT-IN of about 20 S compared to AT-OUT and WT with moderate increases at 13 S and 10 S respectively. The average of multiple experimental repeats indicated a statistically significant salt-dependent increase in sedimentation velocity between AT-IN and WT (P-value = 0.008) and AT-OUT and WT (P-value = 0.024) (Figure 2D). Thus, sedimentation experiments show that the inward bending of the linkers can induce a significantly greater compaction of the nucleosomal arrays than both the WT and the outward bent linker DNAs.

The inward bending of the nucleosome linker promotes nucleosome folding consistent with the 2-start zigzag model

In order to reveal the internal organization of condensed chromatin, we have previously developed and applied EMANIC to resolve nucleosome interactions within compact chromatin fibers (21,22). Here we used partial formaldehyde cross-linking to fix a limited number of internucleosomal contacts (10–30%) in either condensed or decondensed states under the same conditions as described in (21,22); the chromatin is then decondensed at low salt, and TEM is used to provide quantitative assessment of nucleosome-to-nucleosome interactions (Figure 3A) by comparison with non-crosslinked controls. EM images of individual control and crosslinked WT, IN and OUT arrays overlaid with scoring masks for EMANIC are provided in Supplementary EM imaging data files.

Initially, we considered a possibility that the AT-IN configuration with its inward linker DNA bending would promote the solenoid model with primarily i ± 1 interactions. However, we observed significantly stronger i ± 2 interaction for AT-IN arrays in the compact state which corresponds to the zigzag type of packing while AT-OUT arrays have a diffuse pattern of the intra array interactions consistent with less ordered packing (higher deviation) (Figure 3B). Furthermore, AT-IN had significantly more i ± 2 interactions at 150 mM NaCl and 1 mM $MgCl_2$ than the non-cross-linked controls (bottom panel on Figure 3B) with $P = 0.0240$ and $P = 0.0013$, respectively (all P-values are shown in Supplementary Table S2). In contrast, AT-OUT produced almost no additional loops when fixed under monovalent or divalent cation conditions compared to the non-cross-linked controls ($P = 0.2$ and $P = 0.1$, respectively). Specifically, at 150 mM NaCl, AT-IN shows a considerably stronger crosslinking rate or i ± 2 interactions (6.7) compared to AT-OUT (3.0) with $P = 0.006$ (Supplementary Table S2). Thus, consistent with sedimentation coefficient values and TEM images, EMANIC shows that the inward bending of the nucleosome linker, as observed here in AT-IN, promotes nucleosome proximities consistent with the 2-start zigzag chromatin folding model while under the same conditions AT-OUT does not support interactions between the nucleosome cores.

At 150 mM NaCl, the folded WT 12-mer showed notably higher increase in i ± 2 interactions ($P = 0.038$) than AT-OUT but less than AT-IN (Figure 3B). This is consistent with the WT compaction engineered to be intermediate between the AT-IN and AT-OUT (Figure 1C). Interestingly, WT under the same conditions (150 mM NaCl) showed less compact structure than AT-OUT by sedimentation (Figure 2D) despite no significant gain in internucleosomal loops by EMANIC (Figure 3B, central panel). It thus appears that the stiff conformation of the A-tracts (50,53) placed in linker DNA dominates over nucleosome proximities in directing the compactness of the nucleosome array.

Longer oligonucleosome arrays demonstrate the impact of nucleosome linker bending on the longitudinal chromatin fiber compaction

To monitor longitudinal compaction of the nucleosome arrays into 30 nm chromatin fibers that are not observed with the relatively short 12-unit arrays, we also conducted sedimentation velocity and EM imaging with longer, 22-unit (WT and AT-OUT) and 24-unit (AT-IN) nucleosome arrays. As was observed with the 12-mer arrays, sedimentation rates were lowest at low ionic conditions with sedimentation peaks for WT lowest at 38 S, while AT-OUT and AT-IN arrays had sedimentation coefficients at 43 S and 46 S, respectively (Figure 4A and D). Upon the induction of chromatin

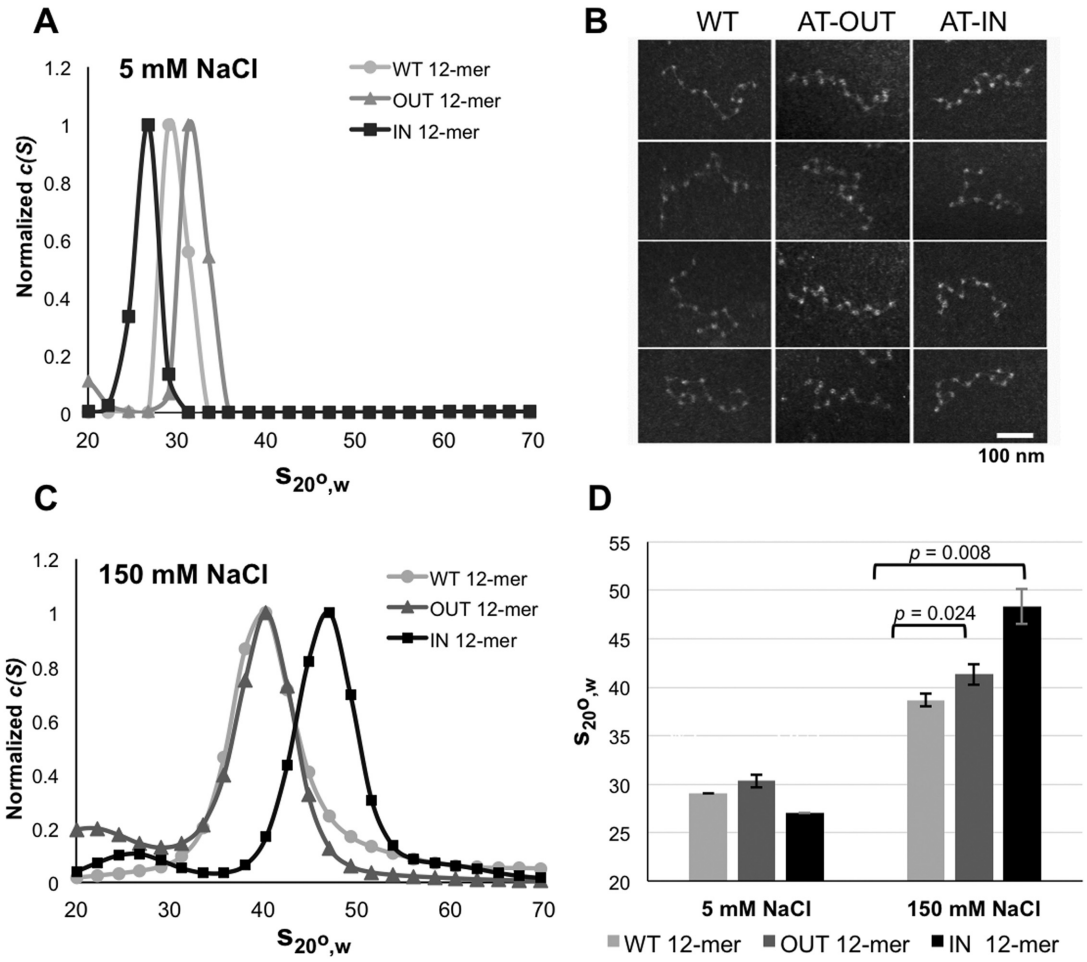

Figure 2. Oligonucleosome array conformation is influenced by linker DNA sequence. (**A**) Distributions of sedimentation coefficients, c(S), for WT and A-tract core arrays in standard HNE buffer (5 mM NaCl). (**B**) Electron micrographs (uranyl acetate staining, dark-field imaging) of WT and A-tract core arrays fixed in HNE with 5 mM NaCl. (**C**) Distributions of sedimentation coefficients, c(S), for WT and A-tract core arrays in HNE with 150 mM NaCl. (**D**) Sedimentation coefficient averages of three independent experiments for WT and A-tract core arrays in HNE with 5 mM NaCl and 150 mM NaCl. Error bars show standard deviations (SD). *P*-values represent probabilities associated with Student's *t*-test.

folding at physiological salt conditions (150 mM NaCl), we observed a significant increase in sedimentation velocity for each array, however, AT-IN increased significantly more (67 S) than both AT-OUT (63 S) and WT (53 S) (Figure 4B). The average of multiple experimental repeats indicated a statistically significant salt-dependent increase in sedimentation velocity between AT-IN and AT-OUT (*P*-value = 0.04) and AT-OUT and WT (*P*-value = 0.008) (Supplementary Figure S4). These results confirm that physiological salt induced a significantly stronger compaction in AT-IN than in both AT-OUT and WT.

Divalent cations are also known to further increase compact folding of nucleosome arrays compared to only monovalent cations, therefore, we tested the chromatin folding effects of 150 mM NaCl plus 1 mM $MgCl_2$ on the longer nucleosome arrays. Here, we observed stronger compaction of AT-IN arrays (to 74 S) while AT-OUT and WT had moderately increased sedimentation values of 67 S and 63 S respectively (Figure 4C and D). The higher degree of compaction of AT-IN at 150 mM NaCl plus 1 mM $MgCl_2$ was statistically significant (*P*-value = 0.029) compared to that of AT-OUT under the same conditions (Supplementary Figure S4). Together with the salt-dependent folding, these data demonstrate AT-IN nucleosome arrays folding capabilities result in tight chromatin structures in the presence of both monovalent and divalent cations.

We then corroborated the results of the sedimentation velocity experiments by TEM imaging. First, nucleosome arrays were fixed at low ionic conditions (5 mM NaCl) and imaged (Figure 5A, left panel). With modest differences in sedimentation velocities, WT, AT-OUT and AT-IN arrays were mostly open and in a 'beads-on-a-string' conformation. A much stronger difference in chromatin compaction was observed at physiological salt conditions (150 mM NaCl) (Figure 5A, right panel). Consistent with EMANIC studies above, AT-OUT arrays had the most open structure still allowing to account for most single nucleosomes in the array. In comparison, AT-IN arrays had tight nucleosome packing as only a few nucleosomes were not included in the compacted chromatin fibers reflecting the highest compaction we observed for sedimentation velocity experiments.

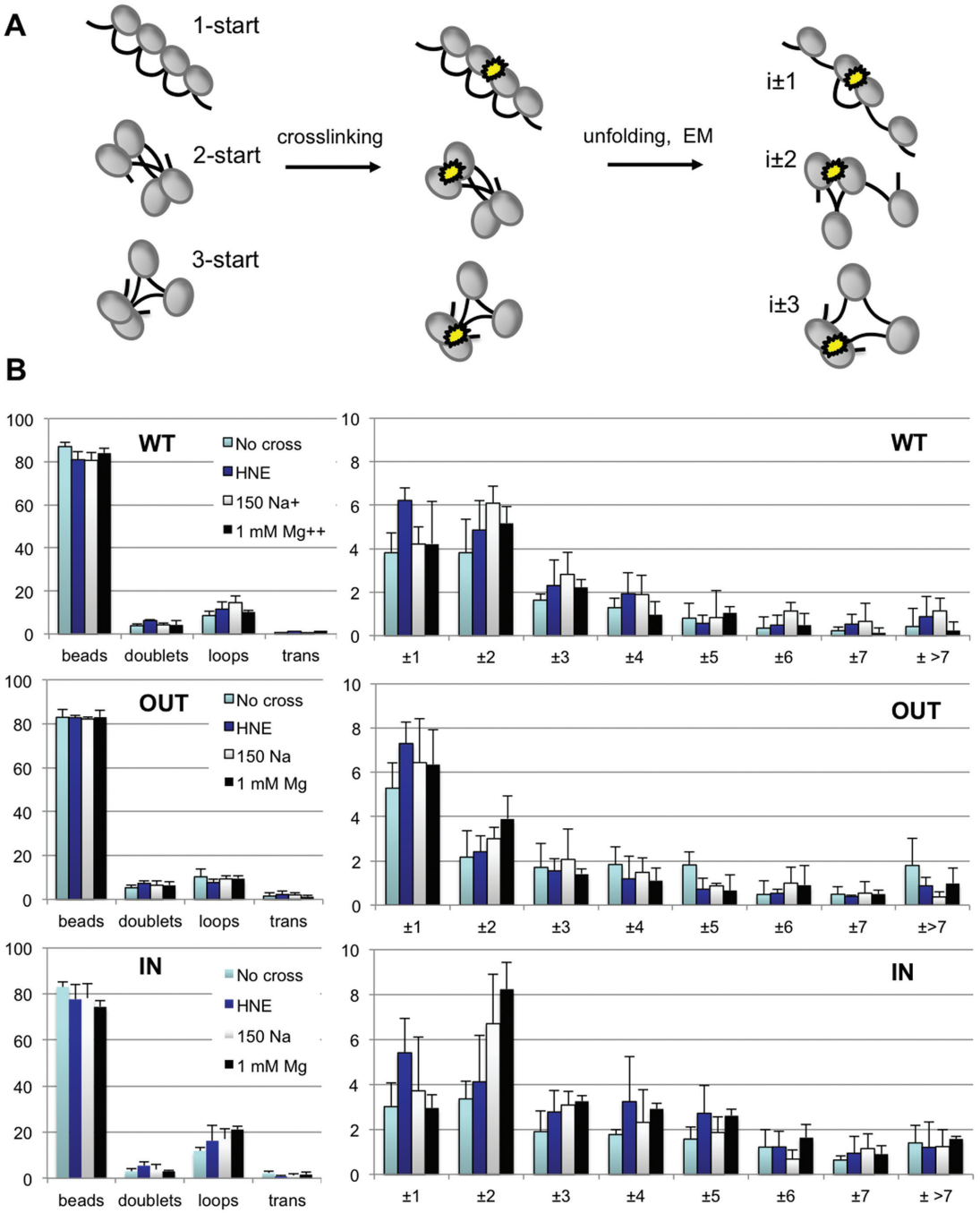

Figure 3. EMANIC analysis of internucleosome interactions in WT, AT-OUT and AT-IN 12-mer nucleosome arrays. (**A**) Scheme of the EMANIC procedure showing nucleosome interactions most frequently observed by EMANIC (21). (**B**) Bar graphs show counting of internucleosome interaction in various conditions after fixing using the EMANIC method. Internucleosome interactions of core nucleosome arrays scored either with or without cross-linking (control) or after formaldehyde cross-linking in the presence of 5 mM NaCl (HNE), 150 mM NaCl or 1 mM $MgCl_2$. Bar graphs on the left (Y-axes) show the total % of nucleosomes involved in no interactions (beads), doublets (i ± 1), loops (i ± 2 or more) and trans interactions (interactions between core arrays). Bar graphs on the right (Y-axes) show the fraction (percentage) of nucleosomes involved in doublet (i ± 1) and loop (i ± 2 to i ± >7) interactions.

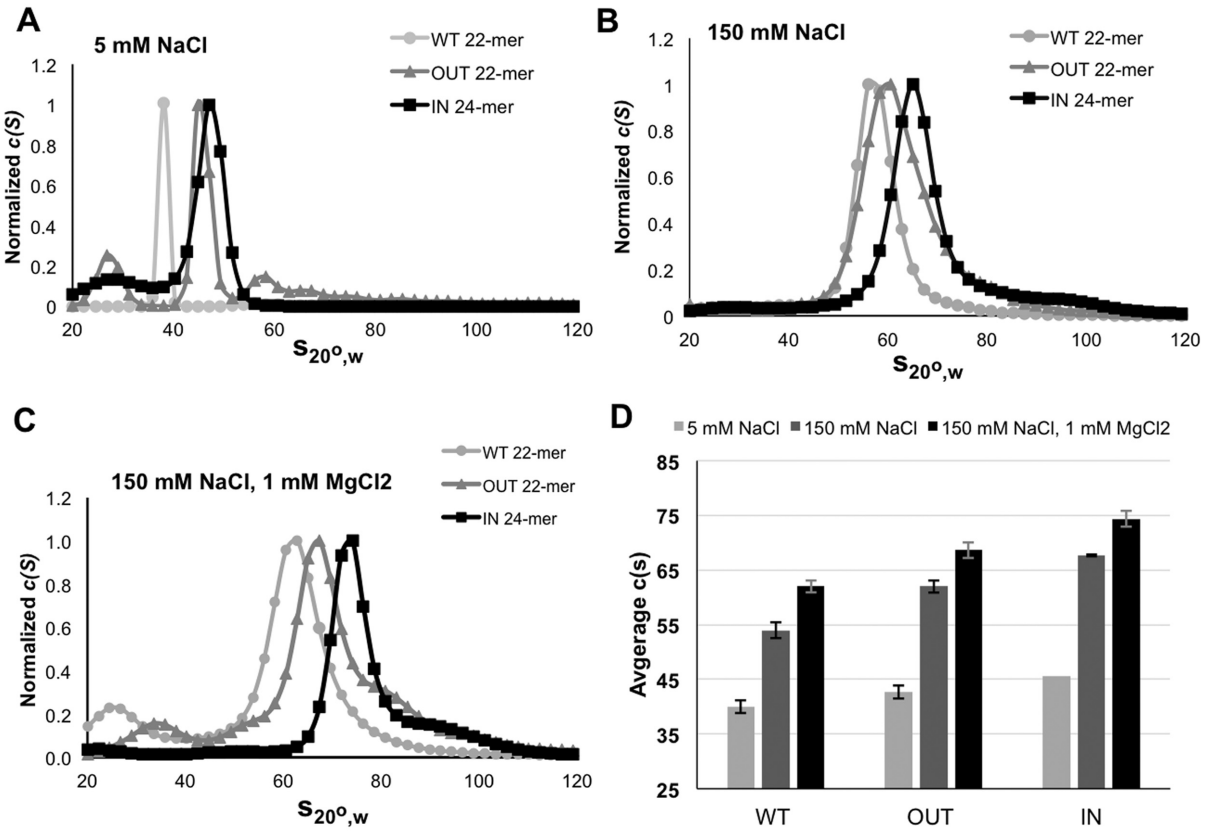

Figure 4. Longer oligonucleosome arrays amplify the impact of A-tract sequences in linker DNA regions. (**A**–**C**) Distributions of sedimentation coefficients, *c(S)*, for WT and A-tract core arrays in HNE buffer with 5 mM NaCl (A), 150 mM NaCl (B) and 150 mM NaCl + 1 mM $MgCl_2$ (C). (**D**) Sedimentation coefficient averages of three independent experiments for WT and A-tract core arrays in HNE buffer with 5 mM NaCl, 150 mM NaCl and 150 mM NaCl + 1 mM $MgCl_2$. Error bars show SD.

TEM images are an excellent tool to physically observe the dimensions of structures that are not measured during sedimentation velocity experiments. In order to quantitate the TEM images of the nucleosome arrays, we measured the average fiber diameters of and the number of nucleosomes per unit length (11 nm) for each construct (Figure 5B and C). At low salt conditions, all three constructs do not show significant differences in compaction and thus, the resulting fiber diameter is similar. The increasing concentration of monovalent cations (150 mM NaCl) lead to notable compaction reflected by a reduced diameter and increased number of nucleosome per unit of length (11 nm) for all arrays. While the particle diameters were significantly higher than 30 nm showing an incomplete folding without linker histone, the number of nucleosome/11 nm (∼3.7) was notably higher in AT-IN than in other arrays. These measurements confirm the AT-IN arrays undergo the strongest longitudinal compaction of the three constructs at physiological ion conditions.

Linker histone H1 induces further compaction of adenine-tract constructs

Linker histone (H1) plays a key role in stabilization of the chromatin fibers by binding closely to the entry/exit point of the nucleosome at the ratio of one molecule per nucleosome (19,54). Here, we used linker histone (H1) isolated from chicken erythrocyte nuclei to reconstitute 12-mer core arrays with one molecule of LH per nucleosome (Supplementary Figure S5A, C and D). Sedimentation velocity experiments with 12-mer arrays showed striking increases in compaction at physiological ionic conditions (150 mM NaCl) with AT-IN showing the highest sedimentation coefficient at 57 S compared to WT and AT-OUT at 51 S and 53 S, respectively (Figure 6A–C).

Linker histone reconstitutes of the longer nucleosome arrays were also generated using one molecule of linker histone per nucleosome (Supplementary Figure S5B and E). As with 12-mers, the 24-nucleosome arrays demonstrate the ability of AT-IN to form a very compact fiber with a sedimentation value of 91 S compared to WT and AT-OUT sedimentation values at 80 S and 82 S respectively (Figure 6D). TEM images of the LH reconstitutes reflect the values observed in sedimentation velocity experiments as AT-IN has apparently thinner chromatin fibers compared to WT and AT-OUT (Figure 6E). Measuring the apparent diameter and length on EM micrographs of the LH arrays shows AT-IN to have a notably smaller diameter than AT-OUT (Figure 6F). Collectively, the comparison of core nucleosome arrays with LH-containing arrays suggests that the latitudinal fiber folding capabilities of LH can synergize with the longitudinal compaction mediated by AT-IN link-

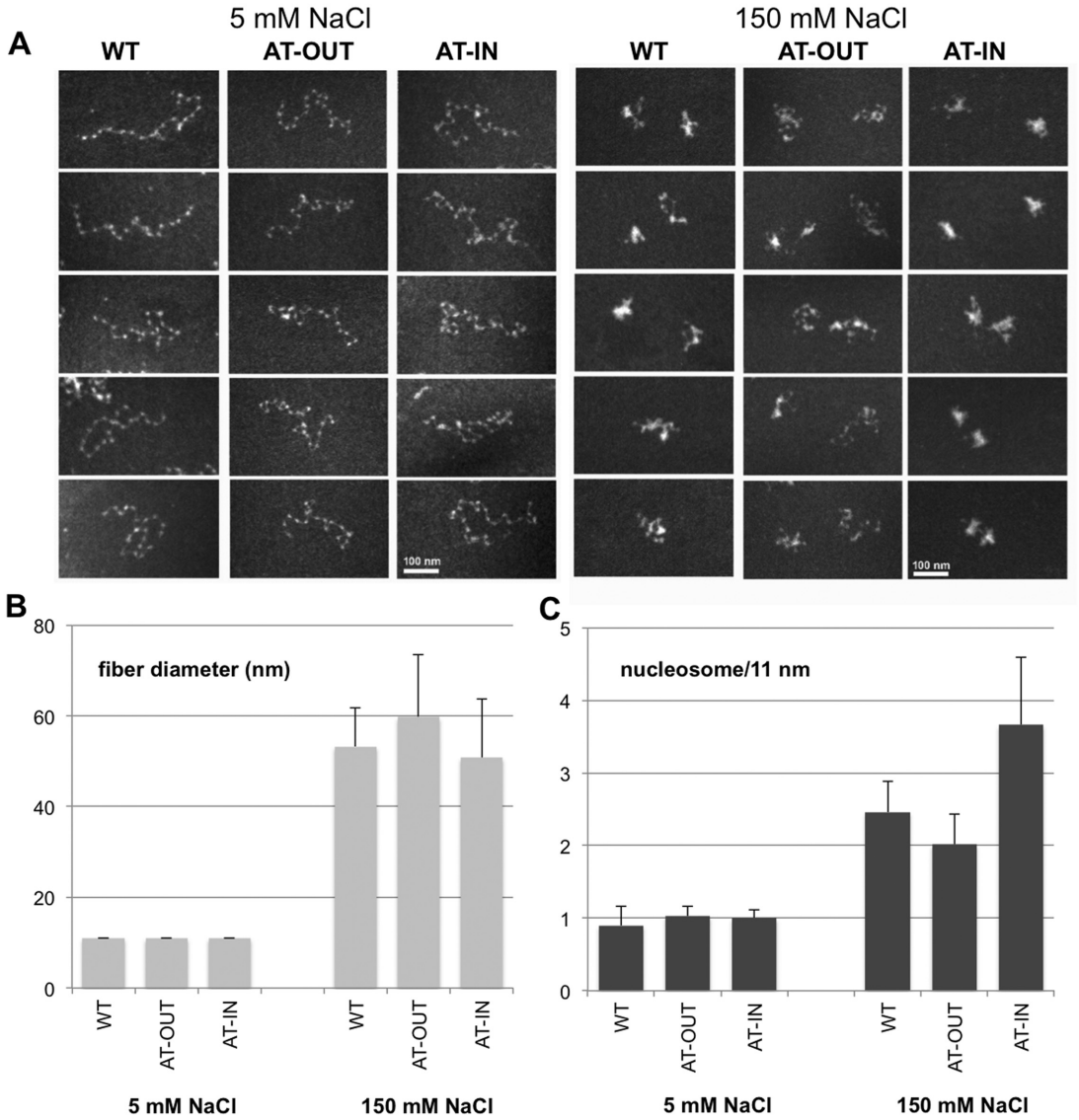

Figure 5. Electron microscopy analysis of the impact of A-tract sequences on chromatin compaction. (**A**) Electron micrograph (uranyl acetate staining, dark-field imaging) of WT and A-tract core arrays fixed in HNE buffer with 5 mM NaCl (left panel) and 150 mM NaCl (right panel). (**B**) Measurements of fiber diameter (nm) of WT and A-tract arrays under the specified conditions. (**C**) Number of nucleosomes per unit length (11 nm) of WT and A-tract arrays under the specified conditions. Error bars: SD.

ers that bring about the highest rate of compaction in the LH-containing AT-IN nucleosome arrays.

Linker DNA accessibility is restricted in AT-IN core arrays compared to AT-OUT

The A-tract constructs were designed to contain repeated (MspI) restriction enzyme sites in linker DNA regions to test the accessibility of these regions when the nucleosome arrays are induced to form compact fibers via monovalent and divalent cations. To probe chromatin conformation, we performed restriction enzyme digestions in the presence of physiological concentration of NaCl (150 mM) and a diluted restriction enzyme buffer (see 'Materials and Methods' section) with only 0.25 mM Mg-acetate to prevent precipitation of the chromatin fibers. The digested nucleosomal DNA was purified by a high-resolution agarose gel electrophoresis. The banding pattern clearly demonstrates faster digestion rate of AT-OUT 22- and 24-mer core arrays by MspI (Figure 7A–C) as also evident by the disappearing main construct band (∼4500 bp) and generation of smaller mononucleosome sized bands (multiples of 189 bp). Overall, AT-IN 24-mer core array has a slower digestion rate by MspI as demonstrated by the remaining main construct band and the lack of mononucleosomes (Figure 7A). The ∼ 2.5-fold higher digestion rate of AT-OUT versus AT-IN nucleosomes (Figure 7D) was confirmed when compared to cleavage of naked 24-mer AT-OUT and AT-IN DNA by MspI (Supplementary Figure S6). Thus, using restriction digestion assays we observed that the inward bending of the linker DNA in the AT-IN arrays is sufficient

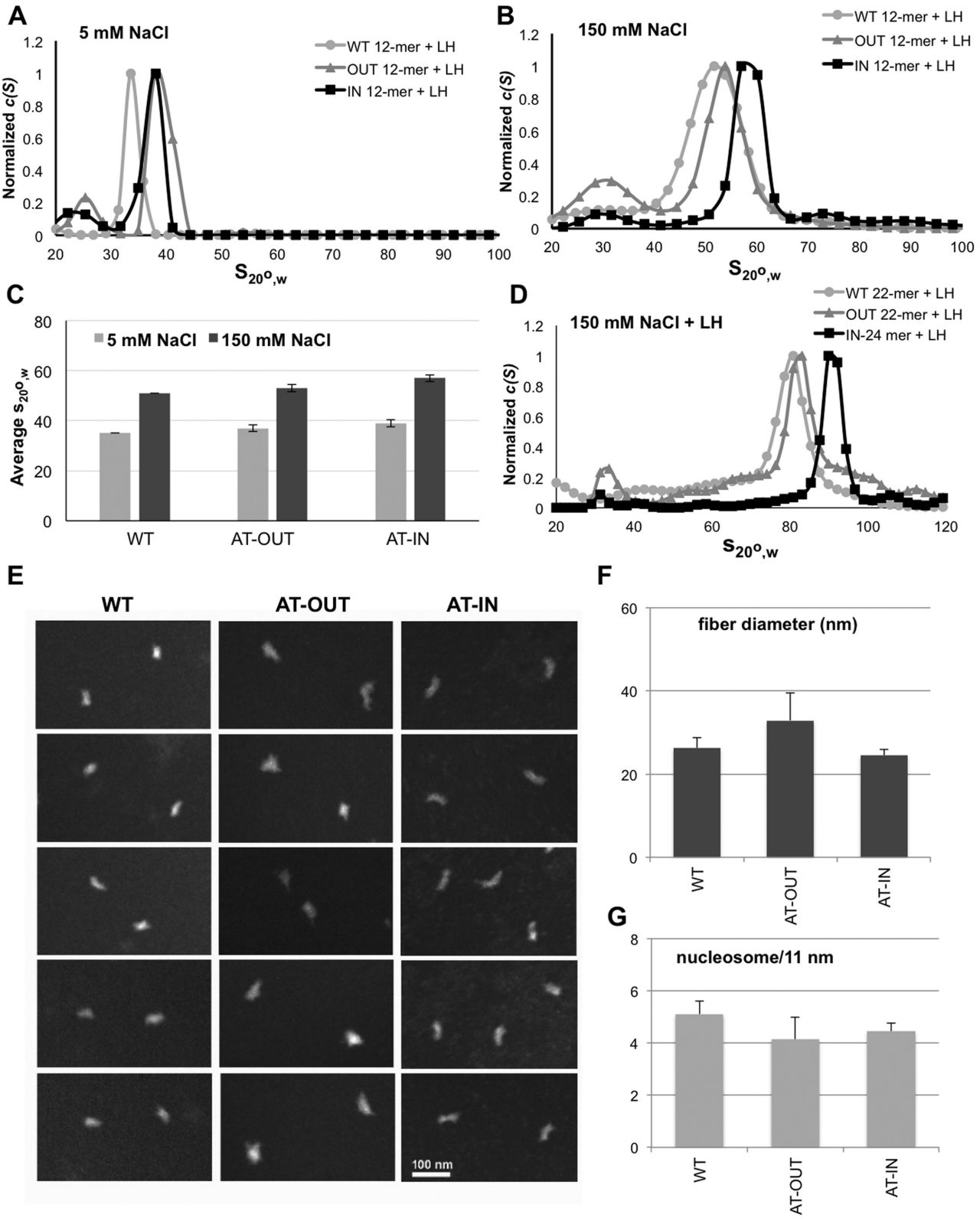

Figure 6. Linker histone H1 promotes compaction of 12-mer A-tract constructs. (**A** and **B**) Distributions of sedimentation coefficients, *c(S)*, for WT and A-tract 12-nucleosome arrays in standard buffer with 5 mM NaCl (A) and 150 mM NaCl (B). (**C**) Averages of sedimentation experiments for WT and A-tract core arrays under 5 mM NaCl and 150 mM NaCl. (**D**) Distribution of sedimentation coefficients, *c(S)*, for WT and A-tract 22–24 nucleosome arrays at 150 mM NaCl. (**E**–**G**) Electron micrographs (E) and measurements of fiber diameter (F) and number of nucleosomes per unit length (G) of WT, AT-OUT and AT-IN nucleosome arrays reconstituted with linker histone H1 and fixed at 150 mM NaCl. Error bars: SD.

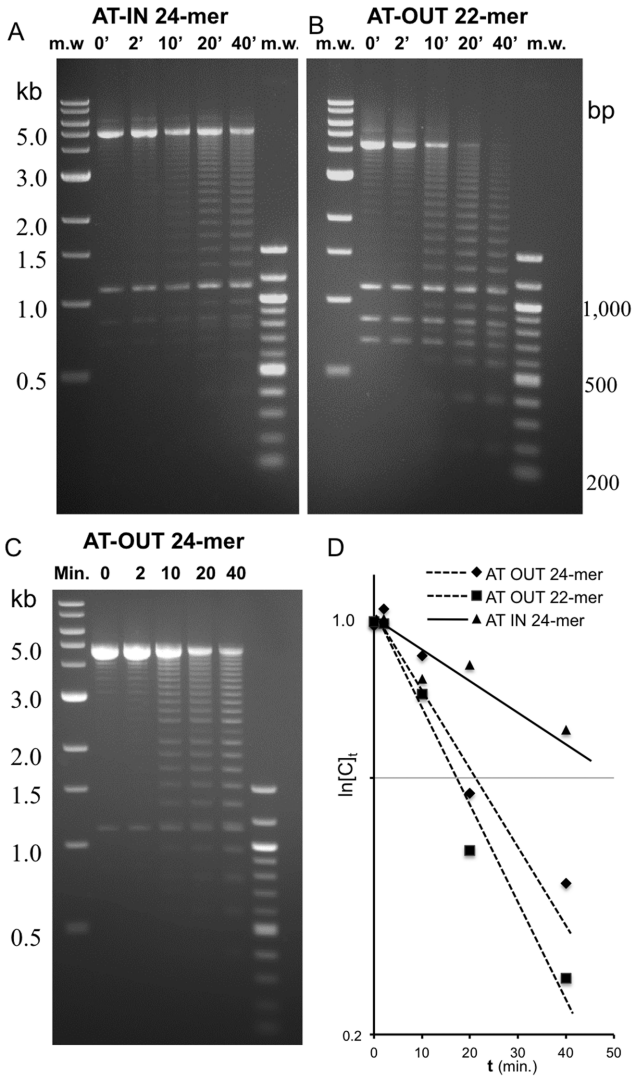

Figure 7. Linker DNA accessibility is more restricted in AT IN core arrays compared to AT OUT. (**A**–**C**) Time course of AT IN 24-mer (A) and AT OUT 22-mer (B) and 24-mer (C) digestion with MspI restriction enzyme. Digestion with this MspI cuts directly in the linker DNA region and results in 189 bp ladder fragments. Each gel shows 1 kb m.w. markers on the left, 100 bp m.w. markers on the right and DNA obtained after RE digestion of reconstituted nucleosome arrays for 0–40 min. (**D**) Graph showing the rate of the intact DNA band decay with linear approximation for the first-order reaction (y-axis shows logarithm (ln) of the normalized intact band concentration) per digestion time (min).

to significantly inhibit DNA accessibility to the restriction enzymes and hence to other DNA-interacting proteins.

3D computational modeling of AT-IN and AT-OUT oligonucleosome arrays

To compare our experimental data with MC simulations of the stereochemically possible conformations of the nucleosome arrays, we designed 3D models of the 12-mer repeats containing the WT, AT-IN and AT-OUT linkers. The three types of nucleosome arrays were constructed as described in 'Materials and Methods' section with invariant nucleosome core structure (PDB ID: 3mvd (44)) and three different linker DNA sequences for WT, IN and OUT given in Figure 1D. Statistical averaging of structural parameters of the system (sedimentation, diameter and rise per nucleosome) was performed for 10 000 MC snapshots (corresponding to 50 million MC steps) taken after the system was equilibrated.

Table 1. MC simulated and experimental sedimentation coefficients for 12-mer arrays

		AT-IN	AT-OUT	WT
Sedimentation $s_{20^\circ,w}$	Experiment	48.3 S	41.3 S	38.7 S
	MC simulation (E = -2.7 kT)	47.6 S	38.6 S	41.4 S
	MC simulation (E = -8 kT)	52.3 S	40.7 S	47.8 S

Shown are sedimentation coefficient averages of three independent experiments for WT and A-tract 12-mer core arrays at 150 mM NaCl and sedimentation coefficient averages calculated after MC simulation of the corresponding 12-mer models. The two sets of MC values are obtained using two different parametrizations of the inter-nucleosome stacking interactions, with the energy −8 kT (27) or −2.7 kT (47).

Monte Carlo simulations predict a substantially more compact equilibrium structure for the AT-IN array (Figure 8) with smaller diameter, reduced length and higher sedimentation velocity then for AT-OUT. The MC simulations are also consistent with the mostly longitudinal compaction of the AT-IN arrays observed by EM (Figure 5A and C). The difference in the diameter shows the same tendency in the experiments and modeling, though the structures appear to be larger by EM. This is not surprising as the diameter is measured in 3D in the model while transmission EM images the oligonucleosome particles flattened on the specimen grid. The MC simulations showing much closer proximity in AT-IN nucleosomes than in AT-OUT nucleosomes are also consistent with EMANIC data (Figure 3) indicating that the AT-IN folds into a 2-start zigzag structure while the AT-OUT configuration does not support internucleosomal interactions under the same conditions.

The two sets of MC values used to calculate sedimentation values were obtained using two different parametrizations of the inter-nucleosome stacking interactions, with the energy −8 kT (27) or −2.7 kT (47). Note that our sedimentation experiments and MC simulations of the AT-IN and -OUT arrays are in a very good agreement (Table 1). A significantly tighter folding of the AT-IN nucleosomes is also consistent with geometry modeling in Figure 1. Importantly, this result does not depend on the parametrization of the nucleosome stacking, even though the predicted sedimentation velocity is systematically higher for the strong stacking (E = −8 kT) than for the weak stacking (E = −2.7 kT), see Table 1. The latter trend is quite natural since the strong inter-nucleosome interactions would preferentially stabilize the compact fiber structures.

Modeling of 12-mer nucleosomes with WT linkers shows somewhat larger deviations from the experiment: the WT oligonucleosomes are predicted by MC simulations (Table 1) to be *more* compact than AT-OUT but appear to be *less* compact than AT-OUT by sedimentation and EM. Appar-

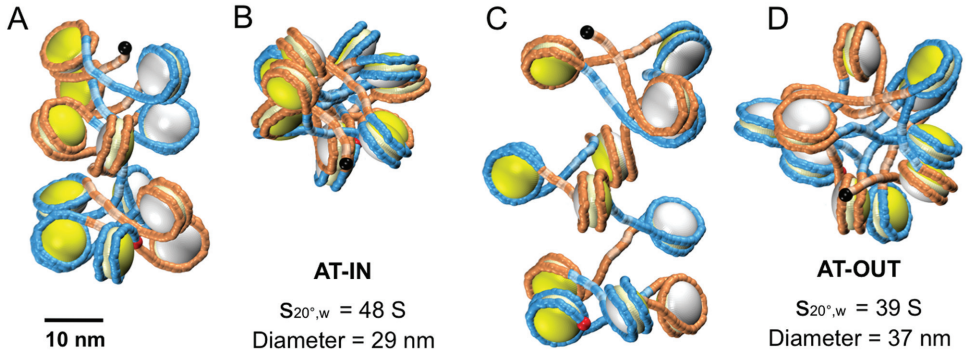

Figure 8. Typical conformations of AT-IN and AT-OUT 12-nucleosome arrays obtained by MC simulations. Models show snapshots representing averaged MC simulations of 12-mer AT-IN (**A** and **B**) and AT-OUT (**C** and **D**) models with the energy −2.7 kT for the inter-nucleosome stacking interactions. Shown are two projections: perpendicular to the main fiber axis (A and C) and along the main fiber axis (B and D). Also shown are predicted sedimentation coefficient ($s_{20}{}^{o}{}_{,w}$) averages and predicted apparent outer fiber diameters calculated by fitting into minimal cylinders. The fiber snapshots shown here were selected so that their predicted sedimentation coefficients are close to the average values observed during MC simulations.

ently, adding the stiffer A-tracts into the linker DNA in the AT-OUT models could make the chromatin fibers more rigid and thus better correspond to the experimental data. Thus, introducing the A-tract into the linkers may generate oligonucleosome arrays most instrumental for testing structural predictions.

DISCUSSION

Structural studies of nucleosomal arrays reconstituted from clone 601 nucleosomal positioning sequence have provided strong evidence for the 2-start zigzag organization of 30 nm chromatin fibers, in which extended DNA linkers are crossed in the middle and nucleosome cores are stacked at the periphery of the chromatin fiber (19,20,54). However, *in situ* imaging (13), as well as nucleosome interaction capture techniques (22,23), have shown that in most cells the chromatin fibers are neither regular nor helical and the nucleosomes show multiple contacts in addition to the predominant 2-start zigzag pattern. The striking discrepancy between the *in vitro* and *in situ* studies is best explained by the variable 3D zigzag model according to which the chromatin structure is heteromorphic and the nucleosome arrays do not form a continuous regular helix due to the variable length and conformation of linker DNA (21,22,24,26).

The zigzag folding of nucleosomes with relatively straight linkers implies that the linker DNA length and 3D configuration should alter the nucleosome orientation in condensed chromatin, thus, regulating chromatin folding by inhibiting and promoting interactions between nucleosome disks. Variations in conformation within nucleosome arrays can be determined by measuring the angle between the entering and exiting linkers of the nucleosome (angle α) and the angle between the flat faces of consecutive nucleosomes (angle β) that is determined by nucleosome linker length (24). Previously in our lab, the effect of angle β on chromatin higher-order structure was demonstrated using nucleosome arrays with various nucleosome repeat lengths (NRLs) matching repeat lengths observed *in vivo* (29). Now, we show that specific nucleotide sequences can alter the DNA geometry, without altering NRL and that the alteration imposed by linker DNA bending (angle α) are sufficient to impact chromatin folding comparable with or exceeding the effect of the NRL (angle β). Furthermore, we show for the first time that the sequence-dependent conformational variability of linker DNA is strong enough to induce a degree of chromatin compaction sufficient to inhibit DNA accessibility to DNA-interacting proteins. Our results thus demonstrate that the variable 3D zigzag model is a potent tool that can predict not only local chromatin higher order structures but also chromatin amenability to the DNA-recognizing factors dependent on spontaneous DNA unfolding (8).

Interestingly, despite the increased DNA curvature in the AT-IN and AT-OUT constructs that could, sterically, promote contacts between nearest neighbor nucleosomes (as it is expected for a solenoidal chromatin models (10)), we have not observed any significant increase of i ± 1 interactions versus control in either AT-IN or AT-OUT constructs by EMANIC (Figure 3B). Accordingly, the MC simulations have not shown any proximity between consecutive nucleosomes (Figure 8) thus strongly arguing against a solenoidal fiber. It should be pointed out that the A-tracks increase the DNA stiffness (55) so that an increased steric proximity between neighbor nucleosomes could be negated by the DNA stiffness.

The eukaryotic genome is wrapped in nucleosomes creating regions of DNA that impede access to most DNA-binding proteins. Several mechanisms are known to contribute to nucleosome positioning *in vivo* such as histone variants, post-translational modifications, higher order chromatin structure, and DNA sequence preferences of nucleosomes themselves (56). The most studied factor of nucleosome positioning is DNA sequence preference, however, nucleosomes form few base-specific contacts between histones and DNA. Nucleosome binding preferences are thought to be determined by the sequence-dependent mechanics of the wrapped DNA itself (57,58). Studies focused on nucleosome preferences consequently found certain DNA motifs that are often excluded from nucleosomes, such as A-tracts (59). The nucleosome exclusion results in a high frequency of A-tracts in nucleosome linkers suggesting not only a role of A-tracts in nucleosome positioning but also in transcriptional regulation as these sites would be available to non-histone DNA-binding proteins. Fur-

thermore, A-tracts are highly enriched in the eukaryotic genomes compared to the prokaryotic genomes suggesting A-tracts play an important role in the eukaryotic genomes (60).

The unique structural and dynamic properties of A-tracts have been shown in an assortment of *in vitro* and *in vivo* assays (reviewed in (50,53)) however an unchartered context for A-tracts is their local and global effect in the genome and the resulting influence on chromatin higher-order structures. The hallmark of A-tracts that has been repeatedly noted is their intrinsic curvature of DNA containing the regularly spaced repeats A_nT_m (summarized in (50)). A-tracts have unusually short helical repeat, 10.0 bp compared to 10.6 bp of typical B-DNA, a distinctively narrow minor groove, and are structurally rigid. These characteristics of A-tracts and their frequent location in the nucleosome linkers indicate A-tracts to be a major contributing factor to the formation of distinct chromatin higher-order structures by influencing chromatin fiber conformation at the primary level. Our results clearly demonstrate the ability of A-tracts to directly affect chromatin fiber structure via DNA linker conformation by altering chromatin folding and nucleosome interaction.

The role of adenine-tracts in regulation of nucleosome occupancy, and gene expression is well established (50,53) so that by manipulating A-tracts position versus promoters, gene expression can be modulated in a predictable manner (61). Our results certainly suggest A-tracts have a strong influence over nucleosome linker conformation that directly impacts chromatin higher order structures and DNA accessibility without altering nucleosome occupancy. Furthermore, A-tracts' high frequency in nucleosome linkers (34,53) and the ability to influence the curvature and stiffness of DNA (55) indicate that A-tracts location in the nucleosome linkers may promote or inhibit chromatin folding and transcription depending on the anisotropic DNA bending toward or away of the chromatin fiber axis. Interestingly, synonymous codon bias restricting A-tract positions has been previously suggested to distinguish exon from non-exon regions at the level of chromatin fiber folding (62) and massive changes in DNA accessibility upon transcriptional induction have been recently shown to occur without changes in nucleosome occupancy (63). We therefore propose that manipulating of A-tract positions in relationship to nucleosomes as well as increasing the number of A-tracts in the linker and/or changing the length of A-tracts could be used as a tool for local alteration of chromatin higher-order structure and DNA site accessibility *in vivo*.

The striking effect of linker DNA bending on chromatin compaction observed here demands a thorough analysis of A-tract position relative to nucleosomes in the genomes to predict the local structural variations of native chromatin. Previous analysis of nucleosome positioning in different genomes such as yeast and chicken revealed an enrichment of A-tracts in the linkers, at positions 0 and −20 in relation to the nucleosome core boundary position (Figure 1A and B) (34). With our construct, these positions clearly conform to the AT-OUT configuration suggesting that the preferred position of A-tracts had evolved to render the nucleosome folding less compact and the DNA more accessible for interaction with external factors. Dramatic changes in NRLs during cell differentiation (64) as well as between active and repressed genes (65) are well documented. It remains to be shown whether the nucleosome relocation can result in shifting the A-tracts to the IN or OUT positions in which they could regulate folding or unfolding of the underlying nucleosomal arrays.

Our finding that the DNA bending can affect chromatin higher order structure poses a question of which other factors could affect DNA bending in the absence of A-tracts. One important factor that is elevated during mitosis and has been shown to increase DNA flexibility and induce interactions between near neighbor nucleosomes is the divalent cation Mg^{++} (66), suggesting that Mg^{++} could specifically increase the folding determined by A-tract configuration. In our experiments, however, adding Mg^{++} increased folding of the AT-IN construct to the same extent as AT-OUT and WT reconstitutes (Figure 4D) indicating that the action of Mg^{++} is not sequence specific.

In the eukaryotic genome, the extent of chromatin fiber folding distinguishes the gene-poor heterochromatin from gene-rich active euchromatin *in vivo* and *in vitro* (7). The A-tracts are present at a minority of nucleosome linkers and, thus, cannot explain the global differences in chromatin compaction. However, additional architectural proteins may induce DNA bending in sequences not enriched with A:T pairs. In living cells, abundant HMGB proteins are known to induce DNA bending are involved in multiple utility functions in the cell and may affect the conformation of linker DNA (67,68). In addition, multiple epigenetic histone modifications and associated architectural factors could alter interactions between nucleosomes and affect chromatin higher order structure (2,4,69). The experimental approaches developed here in combination with recombinant modified histones may further illuminate on whether the natural combination of nucleosome positioning, sequence-specific linker DNA bending, histone modifications and association with DNA architectural factors cooperate to mediate the differences in higher-order folding that distinguish the active and repressed chromatin fibers.

SUPPLEMENTARY DATA

Supplementary Data are available at NAR Online.

ACKNOWLEDGEMENTS

We thank undergraduate interns at Penn State College of Medicine, Hershey: Elizabeth Blaisse and Valentina Kostyuk for experimental assistance. We are thankful to Roland Myers and Han Chen for technical assistance with electron microscopy at the Penn State Hershey Imaging Facility.

FUNDING

NSF grants [MCB-1021681, 1516999 to S.A.G.]; Intramural Research Program of the National Institutes of Health, National Cancer Institute (to V.B.Z.). Funding for open access charge: NSF grant.
Conflict of interest statement. None declared.

REFERENCES

1. Richmond,T.J. and Davey,C.A. (2003) The structure of DNA in the nucleosome core. *Nature*, **423**, 145–150.
2. Tremethick,D.J. (2007) Higher-order structures of chromatin: the elusive 30 nm fiber. *Cell*, **128**, 651–654.
3. Fussner,E., Ching,R.W. and Bazett-Jones,D.P. (2011) Living without 30nm chromatin fibers. *Trends Biochem. Sci.*, **36**, 1–6.
4. Li,G. and Reinberg,D. (2011) Chromatin higher-order structures and gene regulation. *Curr. Opin. Genet. Dev.*, **21**, 175–186.
5. Schlick,T., Hayes,J. and Grigoryev,S. (2012) Towards convergence of experimental studies and theoretical modeling of the chromatin fiber. *J. Biol. Chem.*, **287**, 5183–5191.
6. Luger,K. and Hansen,J.C. (2005) Nucleosome and chromatin fiber dynamics. *Curr. Opin. Struct. Biol.*, **15**, 188–196.
7. Gilbert,N., Boyle,S., Fiegler,H., Woodfine,K., Carter,N.P. and Bickmore,W.A. (2004) Chromatin architecture of the human genome: gene-rich domains are enriched in open chromatin fibers. *Cell*, **118**, 555–566.
8. Zaret,K.S., Lerner,J. and Iwafuchi-Doi,M. (2016) Chromatin scanning by dynamic binding of pioneer factors. *Mol. Cell*, **62**, 665–667.
9. Luger,K., Mader,A.W., Richmond,R.K., Sargent,D.F. and Richmond,T.J. (1997) Crystal structure of the nucleosome core particle at 2.8 A resolution. *Nature*, **389**, 251–260.
10. Thoma,F., Koller,T. and Klug,A. (1979) Involvement of histone H1 in the organization of the nucleosome and of the salt-dependent superstructures of chromatin. *J. Cell Biol.*, **83**, 403–427.
11. Grigoryev,S.A. and Woodcock,C.L. (2012) Chromatin organization—the 30nm fiber. *Exp. Cell Res.*, **318**, 1448–1455.
12. Widom,J. (1989) Toward a unified model of chromatin folding. *Annu. Rev. Biophys. Biophys. Chem.*, **18**, 365–395.
13. Horowitz,R.A., Agard,D.A., Sedat,J.W. and Woodcock,C.L. (1994) The three-dimensional architecture of chromatin in situ: electron tomography reveals fibers composed of a continuously variable zig-zag nucleosomal ribbon. *J. Cell Biol.*, **125**, 1–10.
14. Finch,J.T. and Klug,A. (1976) Solenoidal model for superstructure in chromatin. *Proc. Natl. Acad. Sci. U.S.A.*, **73**, 1897–1901.
15. Kruithof,M., Chien,F.T., Routh,A., Logie,C., Rhodes,D. and van Noort,J. (2009) Single-molecule force spectroscopy reveals a highly compliant helical folding for the 30-nm chromatin fiber. *Nat. Struct. Mol. Biol.*, **16**, 534–540.
16. Worcel,A., Strogatz,S. and Riley,D. (1981) Structure of chromatin and the linking number of DNA. *Proc. Natl. Acad. Sci. U.S.A.*, **78**, 1461–1465.
17. Bednar,J., Horowitz,R.A., Grigoryev,S.A., Carruthers,L.M., Hansen,J.C., Koster,A.J. and Woodcock,C.L. (1998) Nucleosomes, linker DNA, and linker histone form a unique structural motif that directs the higher-order folding and compaction of chromatin. *Proc. Natl. Acad. Sci. U.S.A.*, **95**, 14173–14178.
18. Dorigo,B., Schalch,T., Kulangara,A., Duda,S., Schroeder,R.R. and Richmond,T.J. (2004) Nucleosome arrays reveal the two-start organization of the chromatin fiber. *Science*, **306**, 1571–1573.
19. Song,F., Chen,P., Sun,D., Wang,M., Dong,L., Liang,D., Xu,R.M., Zhu,P. and Li,G. (2014) Cryo-EM study of the chromatin fiber reveals a double helix twisted by tetranucleosomal units. *Science*, **344**, 376–380.
20. Schalch,T., Duda,S., Sargent,D.F. and Richmond,T.J. (2005) X-ray structure of a tetranucleosome and its implications for the chromatin fibre. *Nature*, **436**, 138–141.
21. Grigoryev,S.A., Arya,G., Correll,S., Woodcock,C.L. and Schlick,T. (2009) Evidence for heteromorphic chromatin fibers from analysis of nucleosome interactions. *Proc. Natl. Acad. Sci. U.S.A.*, **106**, 13317–13322.
22. Grigoryev,S.A., Bascom,G., Buckwalter,J.M., Schubert,M.B., Woodcock,C.L. and Schlick,T. (2016) Hierarchical looping of zigzag nucleosome chains in metaphase chromosomes. *Proc. Natl. Acad. Sci. U.S.A.*, **113**, 1238–1243.
23. Hsieh,T.H., Weiner,A., Lajoie,B., Dekker,J., Friedman,N. and Rando,O.J. (2015) Mapping nucleosome resolution chromosome folding in yeast by micro-C. *Cell*, **162**, 108–119.
24. Woodcock,C.L., Grigoryev,S.A., Horowitz,R.A. and Whitaker,N. (1993) A chromatin folding model that incorporates linker variability generates fibers resembling the native structures. *Proc. Natl. Acad. Sci. U.S.A.*, **90**, 9021–9025.
25. Engelhardt,M. (2007) Choreography for nucleosomes: the conformational freedom of the nucleosomal filament and its limitations. *Nucleic Acids Res.*, **35**, e106.
26. Leuba,S.H., Yang,G., Robert,C., Samori,B., van Holde,K., Zlatanova,J. and Bustamante,C. (1994) Three-dimensional structure of extended chromatin fibers as revealed by tapping-mode scanning force microscopy. *Proc. Natl. Acad. Sci. U.S.A.*, **91**, 11621–11625.
27. Norouzi,D. and Zhurkin,V.B. (2015) Topological polymorphism of the two-start chromatin fiber. *Biophys. J.*, **108**, 2591–2600.
28. Wedemann,G. and Langowski,J. (2002) Computer simulation of the 30-nanometer chromatin fiber. *Biophys. J.*, **82**, 2847–2859.
29. Correll,S.J., Schubert,M.H. and Grigoryev,S.A. (2012) Short nucleosome repeats impose rotational modulations on chromatin fibre folding. *EMBO J.*, **31**, 2416–2426.
30. Collepardo-Guevara,R. and Schlick,T. (2014) Chromatin fiber polymorphism triggered by variations of DNA linker lengths. *Proc. Natl. Acad. Sci. U.S.A.*, **111**, 8061–8066.
31. Nizovtseva,E.V., Clauvelin,N., Todolli,S., Polikanov,Y.S., Kulaeva,O.I., Wengrzynek,S., Olson,W.K. and Studitsky,V.M. (2017) Nucleosome-free DNA regions differentially affect distant communication in chromatin. *Nucleic Acids Res.*, **45**, 3059–3067.
32. Koo,H.S., Drak,J., Rice,J.A. and Crothers,D.M. (1990) Determination of the extent of DNA bending by an adenine-thymine tract. *Biochemistry*, **29**, 4227–4234.
33. Nelson,H.C., Finch,J.T., Luisi,B.F. and Klug,A. (1987) The structure of an oligo(dA).oligo(dT) tract and its biological implications. *Nature*, **330**, 221–226.
34. Cui,F. and Zhurkin,V.B. (2009) Distinctive sequence patterns in metazoan and yeast nucleosomes: implications for linker histone binding to AT-rich and methylated DNA. *Nucleic Acids Res.*, **37**, 2818–2829.
35. Lowary,P.T. and Widom,J. (1998) New DNA sequence rules for high affinity binding to histone octamer and sequence-directed nucleosome positioning. *J. Mol. Biol.*, **276**, 19–42.
36. Birnboim,H.C. and Doly,J. (1979) A rapid alkaline extraction procedure for screening recombinant plasmid DNA. *Nucleic Acids Res.*, **7**, 1513–1523.
37. Tan,H.Y. and Ng,T.W. (2008) Acurate step wedge calibration for densitometry of electrophoresis gels. *Opt. Commun.*, **281**, 3013–3017.
38. Springhetti,E.M., Istomina,N.E., Whisstock,J.C., Nikitina,T.V., Woodcock,C.L. and Grigoryev,S.A. (2003) Role of the M-loop and reactive center loop domains in the folding and bridging of nucleosome arrays by MENT. *J. Biol. Chem.*, **278**, 43384–43393.
39. Huynh,V.A., Robinson,P.J. and Rhodes,D. (2005) A method for the in vitro reconstitution of a defined "30 nm" chromatin fibre containing stoichiometric amounts of the linker histone. *J. Mol. Biol.*, **345**, 957–968.
40. Carruthers,L.M., Schirf,V.R., Demeler,B. and Hansen,J.C. (2000) Sedimentation velocity analysis of macromolecular assemblies. *Methods Enzymol.*, **321**, 66–80.
41. Schuck,P. (2000) Size-distribution analysis of macromolecules by sedimentation velocity ultracentrifugation and Lamm equation modeling. *Biophys. J.*, **78**, 1606–1619.
42. Polach,K.J. and Widom,J. (1999) Restriction enzymes as probes of nucleosome stability and dynamics. *Methods Enzymol.*, **304**, 278–298.
43. Schwarz,P.M., Felthauser,A., Fletcher,T.M. and Hansen,J.C. (1996) Reversible oligonucleosome self-association: dependence on divalent cations and core histone tail domains. *Biochemistry*, **35**, 4009–4015.
44. Makde,R.D., England,J.R., Yennawar,H.P. and Tan,S. (2010) Structure of RCC1 chromatin factor bound to the nucleosome core particle. *Nature*, **467**, 562–566.
45. Olson,W.K., Gorin,A.A., Lu,X.J., Hock,L.M. and Zhurkin,V.B. (1998) DNA sequence-dependent deformability deduced from protein-DNA crystal complexes. *Proc. Natl. Acad. Sci. U.S.A.*, **95**, 11163–11168.
46. Zhurkin,V.B., Tolstorukov,M.Y., Xu,F., Colasanti,A. and Olson,W.K. (2005) Sequence dependent variability of B-DNA: an update on bending and curvature. In: Ohyama,T (ed). *DNA Conformation and Transcription*. LANDES Bioscience, Georgetown, pp. 18–34.
47. Funke,J.J., Ketterer,P., Lieleg,C., Schunter,S., Korber,P. and Dietz,H. (2016) Uncovering the forces between nucleosomes using DNA origami. *Sci. Adv.*, **2**, e1600974.

48. Metropolis,N., Rosenbluth,A.W., Rosenbluth,M.N., Teller,A.H. and Teller,E. (1953) Equation of state calculations by fast computing machines. *J. Chem. Phys.*, **21**, 1087–1092.
49. Hansen,J.C., Ausio,J., Stanik,V.H. and van Holde,K.E. (1989) Homogeneous reconstituted oligonucleosomes, evidence for salt-dependent folding in the absence of histone H1. *Biochemistry*, **28**, 9129–9136.
50. Haran,T.E. and Mohanty,U. (2009) The unique structure of A-tracts and intrinsic DNA bending. *Q. Rev. Biophys.*, **42**, 41–81.
51. Nikitina,T., Wang,D., Gomberg,M., Grigoryev,S.A. and Zhurkin,V.B. (2013) Combined micrococcal nuclease and exonuclease III digestion reveals precise positions of the nucleosome core/linker junctions: implications for high-resolution nucleosome mapping. *J. Mol. Biol.*, **425**, 1946–1960.
52. Harp,J.M., Hanson,B.L., Timm,D.E. and Bunick,G.J. (2000) Asymmetries in the nucleosome core particle at 2.5 A resolution. *Acta Crystallogr. D Biol. Crystallogr.*, **56**, 1513–1534.
53. Segal,E. and Widom,J. (2009) Poly(dA:dT) tracts: major determinants of nucleosome organization. *Curr. Opin. Struct. Biol.*, **19**, 65–71.
54. Zhou,B.R., Jiang,J., Feng,H., Ghirlando,R., Xiao,T.S. and Bai,Y. (2015) Structural mechanisms of nucleosome recognition by linker histones. *Mol. Cell*, **59**, 628–638.
55. Drsata,T., Spackova,N., Jurecka,P., Zgarbova,M., Sponer,J. and Lankas,F. (2014) Mechanical properties of symmetric and asymmetric DNA A-tracts: implications for looping and nucleosome positioning. *Nucleic Acids Res.*, **42**, 7383–7394.
56. Segal,E., Fondufe-Mittendorf,Y., Chen,L., Thastrom,A., Field,Y., Moore,I.K., Wang,J.P. and Widom,J. (2006) A genomic code for nucleosome positioning. *Nature*, **442**, 772–778.
57. Zhurkin,V.B. (1983) Specific alignment of nucleosomes on DNA correlates with periodic distribution of purine-pyrimidine and pyrimidine-purine dimers. *FEBS Lett.*, **158**, 293–297.
58. Widom,J. (2001) Role of DNA sequence in nucleosome stability and dynamics. *Q. Rev. Biophys.*, **34**, 269–324.
59. Ozsolak,F., Song,J.S., Liu,X.S. and Fisher,D.E. (2007) High-throughput mapping of the chromatin structure of human promoters. *Nat. Biotechnol.*, **25**, 244–248.
60. Dechering,K.J., Cuelenaere,K., Konings,R.N. and Leunissen,J.A. (1998) Distinct frequency-distributions of homopolymeric DNA tracts in different genomes. *Nucleic Acids Res.*, **26**, 4056–4062.
61. Raveh-Sadka,T., Levo,M., Shabi,U., Shany,B., Keren,L., Lotan-Pompan,M., Zeevi,D., Sharon,E., Weinberger,A. and Segal,E. (2012) Manipulating nucleosome disfavoring sequences allows fine-tune regulation of gene expression in yeast. *Nat. Genet.*, **44**, 743–750.
62. Cohanim,A.B. and Haran,T.E. (2009) The coexistence of the nucleosome positioning code with the genetic code on eukaryotic genomes. *Nucleic Acids Res.*, **37**, 6466–6476.
63. Mueller,B., Mieczkowski,J., Kundu,S., Wang,P., Sadreyev,R., Tolstorukov,M.Y. and Kingston,R.E. (2017) Widespread changes in nucleosome accessibility without changes in nucleosome occupancy during a rapid transcriptional induction. *Genes Dev.*, **31**, 451–462.
64. Weintraub,H. (1978) The nucleosome repeat length increases during erythropoiesis in the chick. *Nucleic Acids Res.*, **5**, 1179–1188.
65. Valouev,A., Johnson,S.M., Boyd,S.D., Smith,C.L., Fire,A.Z. and Sidow,A. (2011) Determinants of nucleosome organization in primary human cells. *Nature*, **474**, 516–520.
66. Tchernaenko,V., Halvorson,H.R. and Lutter,L.C. (2004) Topological measurement of an A-tract bend angle: effect of magnesium. *J. Mol. Biol.*, **341**, 55–63.
67. Malarkey,C.S. and Churchill,M.E. (2012) The high mobility group box: the ultimate utility player of a cell. *Trends Biochem. Sci.*, **37**, 553–562.
68. Bajpai,G., Jain,I., Inamdar,M.M., Das,D. and Padinhateeri,R. (2017) Binding of DNA-bending non-histone proteins destabilizes regular 30-nm chromatin structure. *PLoS Comput. Biol.*, **13**, e1005365.
69. Collepardo-Guevara,R., Portella,G., Vendruscolo,M., Frenkel,D., Schlick,T. and Orozco,M. (2015) Chromatin unfolding by epigenetic modifications explained by dramatic impairment of internucleosome interactions: a multiscale computational study. *J. Am. Chem. Soc.*, **137**, 10205–10215.